Pergamon

Geochimica et Cosmochimica Acta, Vol. 66, No. 10, pp. 1809–1820, 2002

0016-7037/02 $22.00 + .00

PII S0016-7037(01)00893-6

CO_2 in haplo-phonolite Melt: Solubility, speciation and carbonate complexation

Y. MORIZET, R. A. BROOKER, S. C. KOHN*

University of Bristol, Dept. of Earth Sciences, Wills Memorial Building, Queens Rd., Bristol, BS8 1RJ. UK

(*Received February* 21, 2001, *accepted in revised form November* 7, 2001)

Abstract—CO_2 solubility was measured in a synthetic iron-free phonolite (haplo-phonolite) by equilibrating melt with excess CO_2 fluid in a piston cylinder apparatus for a range of pressures (1.0– 2.5 GPa) and temperatures (1300 to 1550°C). The quenched glasses were then analysed using a bulk carbon analytical method (LECO). The measured solubilities are between 0.65 and 2.77 wt.% for the range of conditions studied and show a negative correlation with temperature as reported for most other silicate melt compositions.

A range of carbonate species are present within the glass, as well as minor amounts of molecular CO_2. FTIR and NMR analyses suggest that carbonate is present as both 'network' and 'depolymerised' units as shown for relatively highly polymerised compositions in the model of Brooker et al. (2001b). The bulk CO_2 analyses were used to calibrate the IR extinction coefficient for the carbonate groups. However, the results show that the values obtained for the glasses vary with the melt equilibration conditions, presumably because the ratio of the different carbonate species changes as a complex function of run pressure, temperature and quench rate. Thus the use of IR may not be a reliable method for the quantification of dissolved CO_2 concentrations in natural glasses of 'intermediate' composition. *Copyright © 2002 Elsevier Science Ltd*

1. INTRODUCTION

CO_2 solubility is an important parameter for all models which predict the eruptive behaviour of volcanic systems (e.g. Holloway, 1976; Johnson et al., 1994; Dixon and Stolper, 1995). Even for situations where the concentration is lower than that of water, CO_2 can still play a crucial role in degassing as the lower solubility may result in vesiculation well before water saturation, initiating upward mobility and catastrophic degassing. In addition, CO_2 can have a dramatic effect on phase stability during melting or fractionation, resulting in lavas with unusual compositions (Eggler, 1989).

There have been numerous measurements of CO_2 solubility in natural and synthetic melts (e.g., Mysen et al., 1975, 1976; Mysen, 1976; Rai et al., 1983; Fogel and Rutherford, 1990; Pan et al., 1991; Thibault and Holloway, 1994; Dixon and Stolper, 1995; Dixon, 1997; see review of Blank and Brooker, 1994). Furthermore, it has been shown that CO_2 can dissolve in silicate melts as both molecular CO_2 (CO_2^{mol}) and carbonate (CO_3^{2-}) species (e.g., Brey, 1976; Mysen et al., 1976; Fine and Stolper, 1985; Stolper et al., 1987) and that changes in the silicate species may occur in response to CO_2 dissolution (Verweij et al., 1977; Sharma, 1979; Mysen and Virgo, 1980a, 1980b; Taylor, 1990). In recent years there have been significant advances in our understanding of the CO_2 solubility mechanism and a large number of different species have been identified using NMR and IR spectroscopies and theoretical studies (Kohn et al., 1991; Kubicki and Stolper, 1995; Brooker et al., 1999, 2001a, 2001b). It has also become apparent that natural magmas compositions which are intermediate between acidic rhyolite and basic basalt (e.g., phonolite, trachyte, andesite or dacite) show a transition from molecular CO_2 to carbonate dominated speciation (Fogel and Rutherford, 1990; Brooker et al., 2001b). It is therefore important to investigate these compositions further to determine the relationship between speciation and the compositional dependence of solubility.

CO_2-rich magmas are particularly common in continental rift settings (Bailey, 1980; Bailey and MacDonald, 1987) which have silica-undersaturated, peralkaline volcanic centers. For these alkali-rich magmas, CO_2 is thought to be the essential component controlling Iherzolite phase stability in the mantle source. This results in low-silica, primary compositions such as melilitite and nephelinite (Brey and Green, 1975; Edgar, 1987; Wallace and Green, 1988) which may then fractionate in subvolcanic complexes to give phonolitic compositions. The CO_2-rich nature of these fractionating systems is evident from the common association with carbonatite magmas (Baker, 1987; Le Bas, 1987; Kjarsgaard and Peterson, 1991), the most famous being the active natrocarbonatite volcano, Oldoinyo Lengai (e.g., Bell and Keller, 1995). How CO_2 arrives in the mantle source region is a matter of debate (e.g., Haggerty, 1989), but the idea of a metasomatic agent such as carbonatite melt which stagnates at a thermal ledge and decarbonates to release CO_2 is supported by the unusual trace element enrichment in many nephelinitic-phonolitic systems (Bailey, 1987) and mantle xenoliths (e.g. Coltorti et al., 1999).

However, the presence of mantle xenoliths in phonolitic lavas (Wright, 1966; 1969; Price and Green, 1972; Green et al., 1974), the widespread occurrence of silica-rich, high-alkali glass in xenoliths (e.g., McInnes and Cameron, 1994; Coltorti et al., 1999; Yaxley and Kamenetsky, 1999; Laurora et al., 2001) and the proven stability of such melt compositions in mantle assemblages (Draper and Green, 1997) has highlighted the possibility that some phonolites may be generated directly within the mantle by melting or fractionation.

Cainozoic phonolites erupted in Kenya and Tanzania exceed the total volume of phonolite lava found elsewhere in the world by several orders of magnitude (Lippard, 1973). As well as the phonolites associated with nephelinites in large strato-volcanoes, a second type of phonolite is erupted forming large flood

* Author to whom correspondence should be addressed (yann.morizet@bristol.ac.uk.)

Table 1. Phonolite Compositions in wt.% Oxides

Oxide	Plateau phonolites of Hay and Wendlandt (1995)	Natural, Fe-bearing phonolite from Brooker et al. (2001a)	Haplo-phonolite composition used in this study	Glass analysis for typical sample (YP3, 1500°C and 2.0 GPa)	Glass analysis for sample with residual crystals (YP1, 1300°C and 2.0 GPa)
SiO_2	56.65	57.33	56.84	55.95	56.98
TiO_2	0.56	0.63	0.56	0.57	0.46
Al_2O_3	20.16	19.43	23.04	23.90	22.94
Fe_2O_3	6.01^{tot}	2.85		n/a	n/a
FeO		2.24		n/a	n/a
MnO	0.28	0.17		n/a	n/a
MgO	0.79	1.09	4.08	4.07	4.30
CaO	1.57	2.78	1.58	1.64	1.86
Na_2O	7.84	7.95	13.90	13.87	13.46
K_2O	6.02	5.35		n/a	n/a
P_2O_5	0.12	0.18		n/a	n/a
Total[#]	100.00	100.00	100.00	100.00	100.00
Peralkalinity*	0.963	0.971	0.992	0.955	0.965
NBO/T[$]	0.014	0.039	0.18	0.17	0.19

All analyses recalculated to give a total of 100%.
* defined here as molar $(Na_2O + K_2O)/Al_2O_3$ ratio
[$] Expressed with all Fe as network-former (see Brooker et al., 2001a) and MnO added to MgO. n/a indicates not analysed.

plateaux without evidence of a more basic, or nephelinitic parental composition. It has been suggested that these plateau-type phonolites represent the CO_2 induced melting products of older alkali basalts which 'underplate' the base of the crust. (Hay and Wendlandt, 1995; Kaszuba and Wendlandt, 2000).

Regardless of whether phonolitic magmas represent the ultimate fractionation product of nephelinitic magmas, direct melting of metasomatised mantle or volatile flux melting of underplated crust, they have the potential to experience high activities of CO_2. Saturation in the mantle or lower crust may provide a transport mechanism to the surface. Low confining pressure in shallow level magma chambers and the general trend towards lower solubility in more evolved silicic magmas (e.g. Blank and Brooker, 1994) may lead to saturation at crustal levels. Whether considering eruptive degassing or the thermodynamic activity of CO_2 and its effects on phase relations, it is clear that CO_2 is a highly important component in many phonolitic magmas. A high activity of CO_2 is also a prerequisite for silicate-carbonate immiscibility (Brooker, 1998) and separation from a phonolite is one of the favoured mechanisms for production of the natrocarbonatite erupted at Oldonyo Lengai (Freestone and Hamilton, 1980). Previous studies of CO_2 solubility in natural magmas are limited to a small range of compositions and only three data points are available for phonolite (Brooker et al, 2001a). In this study we use new experimental data to investigate CO_2 solubility in phonolite over a large pressure-temperature range which can be applied to conditions relevant to melting in the mantle or at the base of the crust.

2. EXPERIMENTAL TECHNIQUES

2.1. Starting Materials

The composition chosen for this study is given in Table 1. It is an Fe-free equivalent to the average of the phonolites listed in Hay and Wendlandt (1995). These workers have shown experimentally that CO_2 could have an important role in the genesis of these plateau-type phonolites, if they form by melting of the lower crust. The average natural composition has been modified to remove Fe, Mn and K. The Fe in Hay and Wendlandt (1995) is all listed as Fe_2O_3, but the data of Lippard (1973) suggests this is evenly split (in wt.%) between Fe_2O_3 and FeO in plateau-type phonolites. As a result, the iron has been replaced in equal amounts (in wt.%) by Al_2O_3 and MgO. In addition, the MnO has been replaced by MgO and the K_2O by Na_2O (see Table 1). These substitutions assume that the replacement components will show similar behavior in the melt. The removal of iron and manganese for our simplified composition is an essential pre-requisite for NMR analysis which requires samples free of paramagnetic elements. The absence of iron also removes the experimental difficulties associated with controlling the Fe^{2+}/Fe^{3+} ratio and Fe-loss to the Pt capsules. The K_2O was removed as this may complicate the interpretation of the IR spectra; Brooker et al. (1992) have demonstrated that substitution of the alkali cations in polymerised compositions such as albite or jadeite, can significantly alter the IR doublet of the network carbonates which are observed in the quenched glass.

The Fe-free haplo-phonolite composition was prepared from a mixture of oxides and carbonate, ground under acetone in an agate mortar. Oxides had been previously dried at 1000°C for a few hours and the carbonate at 600°C. An initial Na-free mix was heated at 1300°C to form a partially glassy material and Na_2CO_3 was subsequently added as sources of both Na_2O and CO_2. The glass-carbonate mix is preferred to glass + silver oxalate as this avoids problems of contamination by metallic silver and allows a rapid approach to equilibrium. For NMR samples, the same starting material was prepared with a nominally 99% ^{13}C-enriched Na_2CO_3. Some volatile-free glass was also prepared by melting the Na-bearing mixture at 1400°C. The measured weight loss suggests that only CO_2 is lost during this final melting and all Na_2O is retained.

The starting material was weighed into Pt capsules, and the open capsules were heated in the oven at 110°C, fitted with a lid and then rapidly sealed by arc-welding. Use of this method to reduce the amount of adsorbed water, results in glasses containing less than 0.3 wt. % H_2O.

Two experiments were also performed using the Fe-bearing phonolite starting mix from Brooker et al. (2001a) in $Au_{80}Pd_{20}$ capsules.

2.2. Experimental Apparatus

Experiments were performed in an end-loaded piston-cylinder apparatus using the precautions and pressurisation method reported in Brooker et al. (1998). Temperatures were monitored by a WRe_3-WRe_{25} thermocouple and in all experiments, the capsule was surrounded by an alumina sleeve to avoid contact with the graphite furnace. For the experiments between 1.0 and 2.0 GPa, a 19 mm talc-Pyrex assembly

was used. A tapered graphite furnace was employed to reduce the temperature gradient along the capsule. Measurements with two thermocouples indicated that the thermal gradient is less than 20°C along the 14 mm Pt capsule, (in agreement with Kushiro, 1976). For experiments at 2.5 GPa, a 12.7 mm $BaCO_3$ assembly was used. This assembly also included a tapered furnace giving a thermal gradient of less than 20°C over a 7 mm capsule length. No pressure correction was applied for the talc pyrex assembly, a 13% correction was applied to the $BaCO_3$ cell.

Run durations were at least 2 hours to ensure equilibrium (Mysen et al., 1976). The bulk starting powder contained 9 wt% CO_2 and this produced an excess fluid for all the conditions investigated, as illustrated by a large vesicle at the top of each experimental charge. The temperature quench rate for the piston cylinder apparatus was timed at approximately 100°C/s to 1000°C, falling to around 60°C/s from 1000 to 500°C (below the estimated glass transition temperature). Isobaric quenching ensured that quench (decompression) bubbles were not formed and the glasses are clear and crystal free (unless otherwise stated) with only occasional large vesicles ($>200\mu$m). The diffusion data of Watson (1994) suggests that the amount of the CO_2^{tot} reaching the melt-fluid interface during the quench is insignificant.

2.3. Analytical Techniques

Recovered glasses were analysed for total CO_2 content using a LECO C/S 300 analyser. This involved heating the samples (mixed with iron and tungsten granules) to ~1800°C in a stream of pure oxygen so that all dissolved CO_2 was released. This CO_2 was then analysed with a flow-through infrared cell. The accuracy of the LECO measurements, as determined by relevant calibrations and repeat analyses, was always better than ±0.1 wt.% over the range 0.5 to 3 wt.% total dissolved CO_2, including errors related to any sample inhomogeneity. For most samples, replicate analyses were performed. As the error of the analysis is inversely proportional to the sample mass, the results of replicate analyses were weighted by multiplying the result for each aliquot by the mass, summing and finally dividing by the total mass of sample. A complete listing of analyses for each aliquot, including their masses is given in the Appendix.

Selected sections of glass from the top, middle and bottom of the capsule were analysed by FTIR. Mid-IR spectra were obtained for 100 μm diameter spots through doubly polished plates of glass using a microscope attached to a Nicolet 800 Fourier transform infrared spectrometer operating between 6000 and 650 cm^{-1}. A KBr beamsplitter and MCT detector were used to collect 256 scans at a resolution of 4 cm^{-1} (data points every 2 cm^{-1}). The microscope was enclosed within a box and purged with high purity nitrogen to reduce fluctuations in the atmospheric water and CO_2. The thickness of the sample was measured afterwards by a digital travel gauge with an accuracy of ±1 μm. The thickness of each sample was chosen to give peak intensities below 1.8 absorbance units, as higher values are considered unreliable for quantitative purposes. After the instrumental background was subtracted, the spectrum of a volatile-free haplo-phonolite glass was also subtracted before performing any integrations, leaving CO_2 related peaks as the difference. For some subtractions a linear baseline correction was also applied. The area of the CO_2^{mol} peak at 2351 cm^{-1} and the total area of the carbonate doublet at 1300 to 1670 cm^{-1} were integrated and used for quantitative purposes. Derivation of extinction coefficients also requires a knowledge of the sample density and this was determined for a number of glasses using a Berman balance, weighing the sample in air and in toluene; the precision and accuracy of this technique are within ±1% for samples >10 mg (as determined by measurement of quartz and calcite standards).

The ^{13}C magic angle spinning nuclear magnetic resonance (MAS NMR) spectra were obtained at frequency of 75.432 MHz using a Bruker MSL 300 spectrometer with an external magnetic field of 7.05 T. The chemical shift was referenced to tetramethylsilane (TMS). The area under an NMR peak is directly proportional to the concentration of the species and thus gives direct quantitative information on the $CO_2^{mol}/(CO_2^{mol}$ + carbonate) ratio.

Fragments of glass from some charges were also mounted, polished, and analysed by electron microprobe. Due to the high sodium and volatile content of these glasses it proved difficult to confirm the nominal oxide totals for volatile-free glasses and the correct shortfall for the CO_2-bearing glasses using standard electron microprobe techniques, but the data were internally consistent and samples appeared to be homogeneous. SEM images show no evidence of small bubbles suggesting that the isobaric quenching prevented exsolution.

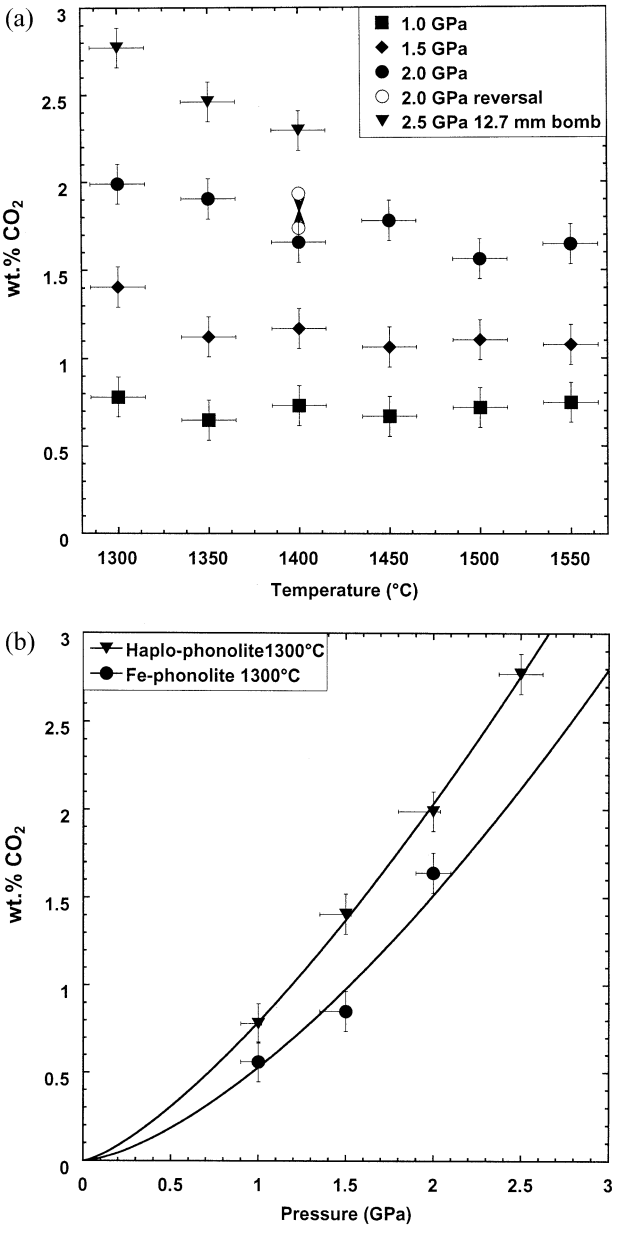

Fig. 1. Experimental solubility data for haplo-phonolite determined using LECO™ bulk carbon analysis. a) The data plotted as a function of temperature. b) The solubility at 1300°C shown as a function of pressure and compared with an Fe-bearing natural phonolite composition (2.0 GPa data point from Brooker et al., 2001a). The solubility error bars include both analytical and experimental error and are based on the standard deviation of the 15 analyses of 5 experiments at 2.0 GPa and 1300°C. The error in temperature is ±15°C determined from measurements of thermal gradient. The estimated error in pressure is +2%/−10% for the 19 mm assembly and ±5% for the 12.7 mm assembly.

Table 2. Solubility Data Obtained by LECO™.

Experiment	Pressure (GPa)	Temperature (°C)	Run duration (h)	Solubility (wt.% CO_2)[a]	Notes
YP12	1.0	1300	2	0.78	
YP34	1.0	1350	3	0.65	
YP10	1.0	1400	3	0.73	
YP35	1.0	1450	3	0.67	
YP07	1.0	1500	3	0.72	
YP39	1.0	1550	3	0.75	
YP11	1.5	1300	3	1.41	
YP31	1.5	1350	3	1.23[c]	^{13}C present
YP09	1.5	1400	3	1.17	
YP32	1.5	1450	3	1.17[c]	^{13}C present
YP06	1.5	1500	2	1.11	
YP33	1.5	1550	3	1.08	
YP01-YP04-YP22-YP27-YP46	2.0	1300	3	1.99[d]	Crystals present
YP28	2.0	1350	3	1.91	Crystals present
YP02-YP66	2.0	1400	3	1.66[d]	
YP20	2.0	1500→1400	6	1.74	Reversal
YP21	2.0	1300→1400	6	1.93	Reversal
YP29	2.0	1450	4	1.78	
YP03	2.0	1500	3	1.56	
YP30	2.0	1550	3	1.65	
YP48[b]	2.5	1300	3	2.77	
YP62[b]	2.5	1350	3	2.46	
YP50[b]	2.5	1400	3	2.29	
YP60	1.5	1300	3	0.85	Fe-phonolite
YP61	1.0	1300	3	0.56	Fe-phonolite

[a] Weighted average of several LECO analyses (see Appendix).
[b] Experiments performed in 12.7 mm assemblies.
[c] Includes 10% correction to account for the presence of ^{13}C in the sample (see text)
[d] Average of several runs (see Appendix)

3. RESULTS

3.1. Solubility Data

CO_2 solubilities measured by LECO bulk analysis are listed along with the run conditions in Table 2 and plotted in figure 1. The value of solubility given for each pressure and temperature is the weighted average of all analyses (as described in section 2.3 and listed in the Appendix). Experiments at 1300°C and 2.0 GPa as well as 1400°C and 2.0 GPa have been replicated to show the possible experimental error (see Appendix). In addition, two reversal experiments were performed to further replicate the 1400°C, 2.0 GPa experiment. In the first of these, the sample was held at 1500°C before lowering to 1400°C. As the solubility at 1500°C is lower (see Fig. 1), this required a significant re-absorption of CO_2 from the excess fluid interface and diffusion into the whole of the charge. This appears to have occurred within 3 hrs. In contrast, the reversal to 1400°C from 1300°C required the exsolution of CO_2 (to form bubbles). This process should be more rapid, but the measured concentration was much higher than the two direct synthesis runs or the other reversal. This may simply be an artifact of the experimental and analytical errors in this study, but super-saturation is observed in basaltic systems at lower pressures (Bottinga and Javoy, 1990) and might be expected as a consequence of this experimental procedure (e.g., Sparks et al., 1994).

For some low temperature runs, small amounts of corundum and spinel were identified (see Table 2) but these minor phases have no measurable effect on the glass composition determined by electron microprobe analysis (Table 1). They are therefore unlikely to have any significant effect on the measured CO_2 solubility. IR spectroscopy showed that two samples which were synthesised from the starting material with the natural abundance of C isotopes, contained ~10% ^{13}C (see Table 2). This suggests that there was some contamination of the Na_2CO_3 starting material for these particular runs, as $Na_2{}^{13}CO_3$ was present in the laboratory. This leads to a potential problem with the LECO analyses, as this instrument is designed to analyze carbon at its natural isotopic abundance. After ensuring that the contribution from any ^{13}C in the LECO analysis is insignificant, a correction of +10% was applied to the measured solubility for these contaminated samples.

Figure 1a shows the solubilities plotted as a function of temperature between 1300°C and 1550°C for each pressure studied. The total range of measured CO_2 solubility in this haplo-phonolite melt is 0.65 to 2.77 wt.%. At 2.5 and 2.0 GPa the solubility clearly decreases with increasing temperature as reported previously for albite (Stolper et al., 1987), diopside (Rai et al., 1983), ol-leucitite (Thibault and Holloway, 1994), and other compositions (Brooker et al., 2001a). However, such a trend is less clearly defined at 1.0 and 1.5 GPa between 1300°C and 1550°C. The data also show an increasing degree of pressure dependence of solubility at lower temperature.

Figure 1b shows the data for 1300°C together with data on the Fe-bearing composition plotted as a function of pressure. It is assumed that the solubility at 0 GPa is 0 wt%, to constrain the form of the pressure dependence. Given the significant dependence of CO_2 solubility on composition, the results for the natural, Fe-bearing phonolite (1.0 and 1.5 GPa this study, 2.0

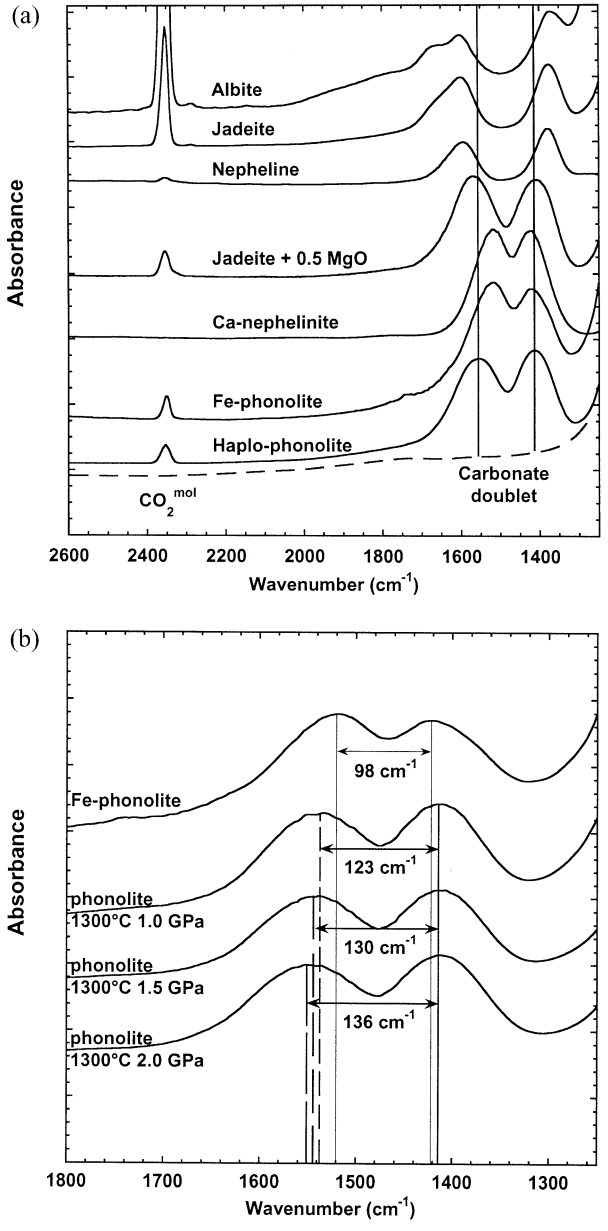

Fig. 2. a) The FTIR spectrum of haplo-phonolite (this study) compared with spectra of other selected compositions (Brooker et al., 1999; 2001b). The spectra represent samples of different thickness but are scaled for optimal presentation. The spectrum of a volatile-free haplo-phonolite is shown as a dashed line. b) The variation in the carbonate doublet splitting (from 123 cm^{-1} to 136 cm^{-1}) for three haplo-phonolite samples synthesised at 1300°C but at different pressures (1.0, 1.5 and 2.0 GPa). This is compared with the carbonate splitting for the Fe-bearing phonolite which is 104 cm^{-1}.

GPa from Brooker et al., 2001a) are in reasonable agreement with the haplo-phonolite, following a similar trend, but with 25 to 30% lower solubility. The slightly lower solubility may result from the lower NBO/T of the natural composition (Table 1) consistent with the NBO/T relationship noted by Brooker et al. (2001a), an interpretation which holds true whether or not Fe^{2+} and Fe^{3+} are assigned to network forming or network modifying roles (see Mysen, 1988). Alternatively the lower solubility could be due to the lower Al/Si ratio in the natural compositions (Table 1) as this ratio is known to significantly affect solubility in polymerised compositions along the albite-jadeite-nepheline join (Brooker et al., 1999). Similar arguments may explain the similarity between CO_2 solubilities for the haplo-phonolite and those reported for tholeiite at 1.0 and 1.5 GPa (Pan et al., 1991), even though the NBO/T of tholeiite is significantly higher (0.34 vs. 0.18). The relative importance of NBO/T and Al/Si in controlling solubility is related to the nature of the carbonate groups which may be present, as discussed below.

3.2. Infrared Results

A typical mid-IR spectrum of the haplo-phonolite is shown at the bottom of Figure 2a and compared to spectra for other selected compositions. In this figure, the molecular CO_2 peak is located at about 2351 cm^{-1} (Fine and Stolper, 1985; Brooker et al., 1999) and is slightly asymmetric. Carbonate species are represented by a complex doublet between 1670 and 1300 cm^{-1} (Fine and Stolper, 1985; Brooker et al., 1999). The haplo-phonolite and the natural Fe-phonolite glasses both show a $CO_2^{mol}/(CO_2^{mol}$ + carbonate) ratio which is intermediate in character between more basic compositions such as basalt or nephelinite, which contain only carbonate (Fine and Stolper, 1985), and more acidic compositions, such as rhyolite which contain only molecular CO_2 (Fogel and Rutherford, 1990).

The other distinguishing feature of the IR spectra of carbonate-bearing glasses is the value of $\Delta\nu_3$, the splitting of the ν_3 carbonate doublet, which is thought to reflect the distortion experienced by carbonate groups in different configurations (Blank and Brooker, 1994; Brooker et al., 2001b). The splitting is highest in nominally fully polymerised compositions (NBO/T = 0) due to the presence of highly distorted 'network' carbonates (T-carb-T) where two of the carbonate oxygens are shared with the Si and/or Al tetrahedra which form the aluminosilicate framework (Fine and Stolper, 1985; Kohn et al, 1991; Kubicki and Stolper, 1995; Tossell, 1995). Brooker et al. (1999, 2001b) suggested that $\Delta\nu_3$ for these network carbonates increases from 225 cm^{-1} for Al-carb-Al groups, to 295 cm^{-1} for Si-carb-Si. The change in the relative importance of these groups as a function of the bulk Al/Si ratio can be seen for Ab, Jd and Ne in Figure 2a. A smaller $\Delta\nu_3$ of 80 to 90 cm^{-1} is observed in most depolymerised natural compositions such as the Ca-nephelinite (Fig 2a), and is thought to represent a less distorted carbonate group which is linked to the framework via a non-bridging oxygen (represented as NBO-carb by Brooker et al., 2001b). The $\Delta\nu_3$ for haplo-phonolite is somewhat different from the natural phonolite composition (Fig. 2a). The splitting for the natural phonolite is only slightly wider than that of depolymerised compositions such as Ca-nephelinite ($\Delta\nu_3$ of 101 ± 3 vs. 80 cm^{-1}), but the split for the haplo-phonolite ($\Delta\nu_3 \sim 130 \pm 7$ cm^{-1}) is intermediate between depolymerised and fully polymerised compositions. Furthermore the high frequency edge of the doublet for both phonolite compositions extends to much higher frequency than for Ca-nephelinite.

Also shown in Figure 2a is a spectrum for the composition Jd + 0.5MgO from Brooker et al. (2001b). This composition represents the depolymerisation of Jd (NBO/T = 0) by addition of 0.5 moles of MgO. The resulting NBO/T of 0.167 and MgO

content of 4.75 wt% are very similar to the haplo-phonolite of this study. Brooker et al. (2001b) noted that the ν_3 splitting for Jd + 0.5MgO was surprisingly wide ($\Delta\nu_3$ = 168 cm^{-1}) compared to Jd depolymerised by an equivalent molar amount of CaO ($\Delta\nu_3$ = 70 cm^{-1}) as well as other depolymerised compositions. These authors suggested that a Mg-carb-T network carbonate might be responsible, having a distortion intermediate between Al-carb-Al which is dominant in Ne (Fig. 1a), and the NBO-carb observed in other depolymerised compositions. It is not possible to simulate the haplo-phonolite in Figure 2a by combining the spectra of Ne and a highly depolymerised composition, but the $\Delta\nu_3$ and characteristic shape can be simulated by a 25/75 mixture of the spectra for Ca-nephelinite and Jd + 0.5MgO. The relatively high MgO concentration in the haplo-phonolite compared with the natural phonolite composition could therefore explain the larger splitting and wider base to the carbonate doublet in the IR spectra.

Compared to the natural Fe-bearing phonolite, the haplo-phonolite carbonate doublet also appears to have a more equal intensity for the two doublet peaks. Brooker et al. (2001b) have suggested that the higher intensity of the 1550 cm^{-1} peak in the natural composition might be due to an additional single peak component at 1460 cm^{-1} which is a feature of highly peralkaline compositions. Although the 'peralkalinity' (as defined in Table 1) is very similar for these two compositions, any Mg assigned to tetrahedral coordination (as suggested above) may also require Na to charge balance, effectively reducing the peralkalinity in the haplo-phonolite.

A more subtle feature of the carbonate doublet is shown in Figure 1b which illustrates the spectra obtained for haplo-phonolite synthesised at different pressures. The separation of the two peak maxima changes from 136 cm^{-1} to 123 cm^{-1} possibly reflecting a change in the relative abundances of different types of carbonate groups (e.g. Mg-carb-T vs. NBO-carb groups) for glasses quenched from different run conditions.

It should be noted that none of the IR (or NMR) spectra of samples included in this study showed any detectable evidence of reduced carbon species such as CO or CH_4 which would result from diffusion of hydrogen through the capsule (from the dehydration of the talc assembly parts). Samples prepared during the course of this study which did show evidence of hydrogen infiltration were not used in the solubility dataset.

3.3. NMR Results

Three ^{13}C enriched samples synthesised at 2.0 GPa and 1300°C, 1350°C and 1550°C were analysed by NMR and are shown in Figure 3a. The narrow peak at 125 ppm is assigned to CO_2^{mol} and the broad asymmetric resonance at 150 to 170 ppm is assigned to carbonate (Kohn et al., 1991; Brooker et al., 1999). There is a small but significant variation in the proportion of CO_2^{mol} decreasing from 4 ± 1% at 1300°C, to 3 ± 1% at 1350°C and 2.2 ± 1% at 1550°C. A similar change in $CO_2^{mol}/(CO_2^{mol}+\text{carbonate})$ with run temperature has been observed for other compositions (Stolper et al., 1985; Brooker et al., 1999). This effect would not normally be predicted, given the relatively constant quench-rate (and T_g) for all run temperatures (see section 3.4).

Figure 3b shows the carbonate spectrum for the haplo-phonolite compared to a more depolymerised composition (sodamelilite) and the fully polymerised composition nepheline. The haplo-phonolite clearly shows intermediate behaviour consistent with the observations made using the IR spectra. The asymmetry of the broad carbonate peak indicates that there is more than one type of carbonate present in this composition. Figure 3c shows a four peak fit for the carbonate peak of the 1300°C, 2.0 GPa sample. The shifts of the fitted peaks are 168.4, 165.3, 160.5 and 155 ppm, with widths of 4.6, 5.9, 5.6 and 6.0 ppm and areas of 35.3, 54.7, 8.6 and 1.4% respectively. To obtain this fit the positions, widths and intensities of 3 peaks were completely free but a small peak at 155 ppm with a fixed width and intensity was forced to be present to satisfactorily fit the low frequency tail. A fit of the carbonate region for the 1550°C and 2.0 GPa sample gives similar results within error. The lack of resolution in the spectra means that these fits are not unique, but they do provide one possible solution which can be compared with IR data of other samples. If more than four different types of carbonate are present in this complex multi-component composition, it is unlikely that any detailed information could be extracted from fitting the spectra.

Brooker et al. (1999) have observed peaks with similar shifts in nominally fully polymerised compositions such as albite, jadeite and nepheline. The 165 ppm peak was assigned to the network carbonate species Al-carb-Al, the 160 ppm to Si-carb-Al and the 155 ppm peak to Si-carb-Si. As noted in section 3.2 the IR spectra for the haplo-phonolite is clearly not a simple mixture of the network carbonate groups present in Ab, Jd and Ne, together with the NBO-carb groups of depolymerised compositions such as Ca-Nephelinite; the fact that peaks close to 165, 160 and 155 ppm are found for the phonolite glass is therefore probably a coincidence. The NMR spectrum for the carbonate in the Jd + 0.5MgO composition is not available, so it is not known if the 165 and 160 ppm components (or some other fitted peaks) might be related to the Mg-carb-T group. The 168 ppm peak is probably related to NBO-carb which is dominant in more depolymerised composition such as sodamelilite (NBO/T = 0.67) in Figure 3b. This is consistent with the IR data and the conclusions of Brooker et al. (2001a, 2001b) who suggested that the dissolution mechanism of CO_2 for highly (but not fully) polymerised compositions such as phonolite would involve both 'network' and 'depolymerised' carbonate species.

4. DISCUSSION

4.1. Thermodynamic Treatment of Solubility Data

One way to model CO_2 solubility over a wide range of P, T conditions is to develop a thermodynamic model based on a limited number of experimental data points, then derive key parameters such as K, ΔH and ΔV for the given composition. Simple thermodynamic models have been developed for rhyolite (Fogel and Rutherford, 1990), tholeiite (Fine and Stolper, 1985; Stolper and Holloway, 1988; Pan et al., 1991), and ol-leucitite (Thibault and Holloway, 1994). Based on the spectra for quenched glasses, the haplo-phonolite presented in this study appears to be dominated by carbonate species (>96%), and to make a comparison with the data of previous authors we have attempted to model our data assuming the solubility mechanism can be described by the following reaction:

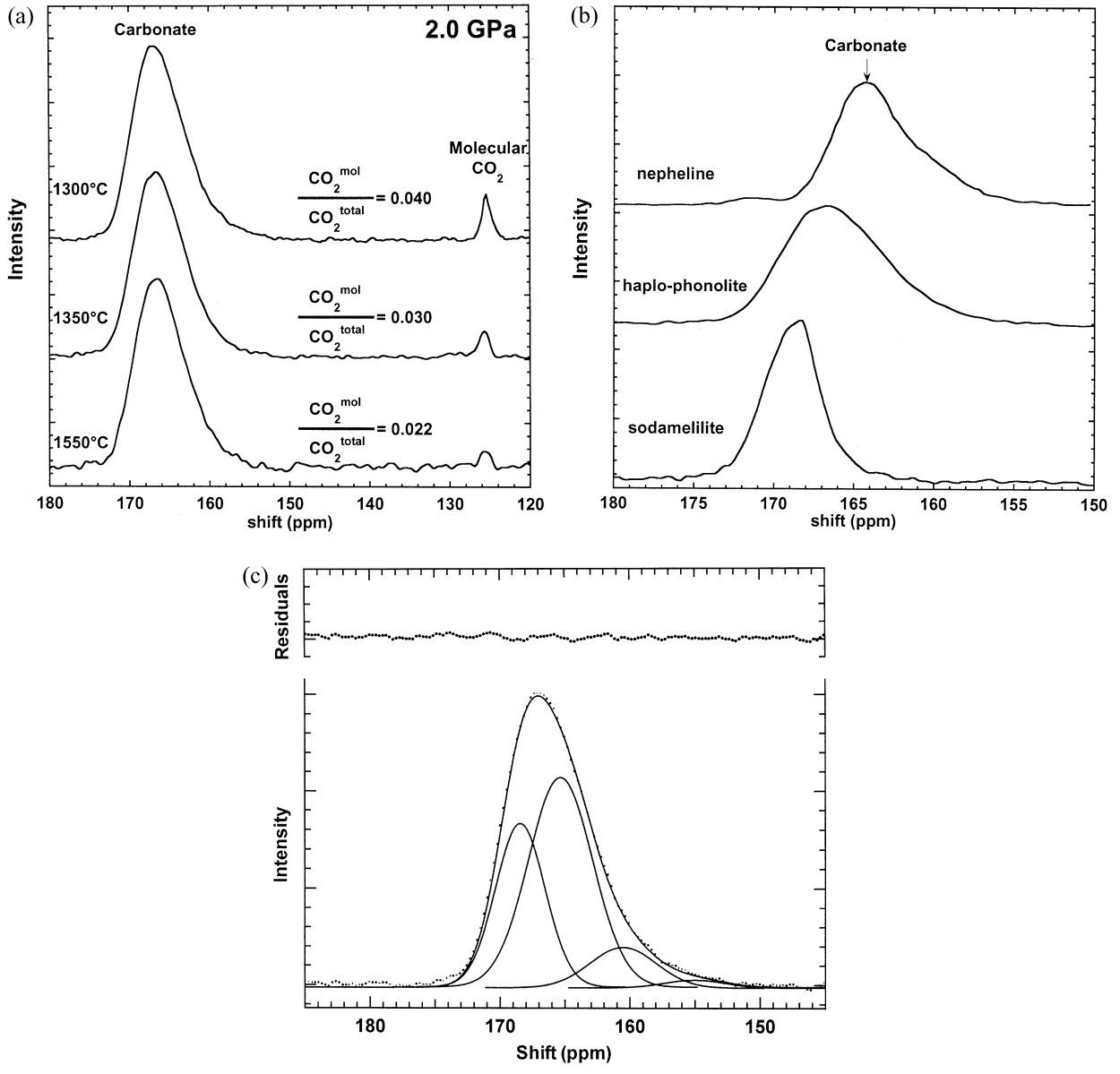

Fig. 3. a) NMR spectra of three haplo-phonolite samples showing the change in $CO_2^{mol}/(CO_2^{mol}$ + carbonate) as a function of run temperature at 2.0 GPa. b) Comparison of the carbonate region of haplo-phonolite glass with spectra for other compositions. The width and position of the peak for phonolite (NBO/T = 0.18) are intermediate between that for nepheline (NBO/T = 0) and sodamelilite (NBO/T = 0.67). c) The results of fitting the carbonate region of the NMR spectrum of the 1300°C sample with 4 Gaussian peaks. The dotted curve is the experimental spectrum, solid lines are the fitted Gaussians and their sum, the upper line is the residual.

$$CO_2^{(fluid)} + O^{2-(melt)} \overset{K}{\rightleftharpoons} CO_3^{2-(melt)} \quad (1)$$

The corresponding equation for this reaction as a function of pressure, temperature and thermodynamic parameters is:

$$\frac{X^{(m)}_{CO_3^{2-}}}{X^{(m)}_{O^{2-}} * f(CO_2)} = K^0 * \exp\left[\frac{-\Delta V^0}{R*T}*(P - P^o) - \frac{\Delta H^o}{R} * \left(\frac{1}{T} - \frac{1}{T^0}\right)\right] \quad (2)$$

Where:

$X_i^{(m)}$ is the molar fraction of the i species in the melt (this is approximately equal to the activity if ideal mixing is assumed).

ΔH^0 and ΔV^0 are the change in molar enthalpy and molar volume.

K^0 is the equilibrium constant for Eqn. (1) at P^0 and T^0.

P^0 and T^0 are chosen as 0.1 GPa and 1473°K respectively.

$f(CO_2)$ is the fugacity of CO_2 in bars in the fluid phase.

Using Eqn. (2) it is possible to obtain best fits for the different thermodynamic parameters using the entire haplo-phonolite solubility data set in Figure 1. This data set is

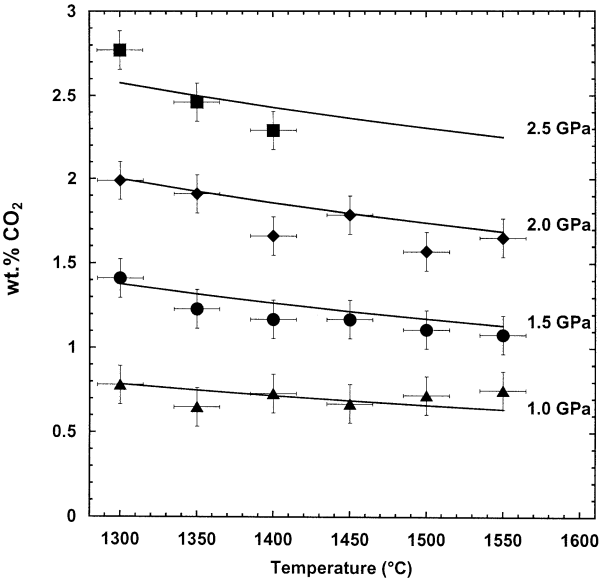

Fig. 4. Modeling of the CO_2 solubility data for the haplo-phonolite following the thermodynamic method of Pan et al., (1991). The lines represent the best fit to the experimental data according to the parameters given in Table 3.

reproduced in Figure 4 along with lines calculated using these 'best fit' parameters. Values for K^0, ΔH^0 and ΔV^0 are listed in Table 3 and are compared to values obtained for tholeiite and ol-leucitite. Note that we have calculated the fugacity of CO_2 using the equation of state of Frost and Wood (1995), whereas the studies of tholeiite and ol-leucitite used the equation of state of Saxena and Fei (1987), but over the P/T range investigate here there is no significant difference in the values obtained with either method. The values of ΔV^0 and ΔH^0 take into account the pressure and temperature dependence respectively. The similar values for ΔV^0 suggests that the pressure dependence of the CO_2 solubility is similar in all compositions. The intermediate ΔH^0 value implies a temperature dependence intermediate between those for tholeiite and ol-leucitite. However, the model does not appear to accurately predict the variation in temperature dependence as a function of pressure (Fig. 4). One mechanistic explanation for the failure of the model could involve the fact that there are several carbonate groups present (as shown by the spectroscopic data), each with unique values of K^0, ΔH^0 and ΔV^0 and that the relative abundances of these groups in the glass may reflect changes in the melts equilibrated over a range of P and T (Fig 2b). It is also possible that the molecular CO_2 species plays a more important role in the melt, but is converted to carbonate during quenching (see section 4.3).

Table 3. Thermodynamic Parameters for Carbonate Dissolution

Parameters	Haplo-Phonolite (this study)	Tholeiite (Pan et al., 1991)	Ol-Leucitite (Thibault and Holloway 1994)
ln K^0	−15.04	−14.83	−13.36
ΔH^0_r (kJ.mol^{-1})	−17.21	5.2	−28.15
ΔV^0_r (cm^3.mol^{-1})	22.77	23.14	21.53

All parameters were calculated using the method described by Pan et al. (1991) and Thibault and Holloway (1994) using $P^0 = 0.1$ GPa and $T^0 = 1473$°K as the standard state.

It should be noted that if taken literally, Eqn. (1) implies a reaction between CO_2 and a free oxygen (O^{2-}), even though the abundance of free oxygen in glasses is known to be extremely low for relatively polymerised compositions such as phonolite (Maekawa et al., 1991; Yokokawa et al., 1999). In fact, it is not clear which types of oxygen are actually involved in the dissolution mechanisms, with non-bridging oxygens (O^-) favoured for reaction to produce NBO-carb and bridging oxygens (O^0) for network carbonate. When complex rearrangements of the silicate structure are also considered, it is unlikely that a reaction as simple as Eqn. (1) will be adequate for intermediate compositions such as phonolite.

4.2. IR Extinction Coefficients

FTIR is often used to investigate the concentration of various dissolved volatile species in glasses using the Beer-Lambert approximation:

$$C = \frac{MW \times abs}{\rho \times d \times \varepsilon} \quad (3)$$

where C is the concentration, MW is the molecular weight, abs is the peak intensity or area, ρ is the glass density (g.L^{-1}), d the thickness of the sample (cm) and ε is the extinction coefficient (L.mol^{-1}.cm^{-2} for the integrated area, L.mol^{-1}.cm^{-1} for the peak height). The extinction coefficients for dissolved CO_2 species are known to be composition dependent (e.g., Ihinger et al., 1994; Dixon and Pan, 1995; Brooker et al., 1999) and thus require calibration for each composition.

In this study we have bulk solubility data from LECO analyses and quantitative speciation data from NMR spectra, therefore the IR extinction coefficients for both CO_2^{mol} and carbonate species can be calculated if the glass density is known. Densities were determined for glasses quenched from 1.0 GPa (1350, 1450 and 1550°C) and fall within the range 2498 to 2501 g.L^{-1}, those at 1.5 GPa (1300, 1350, 1450 and 1550°C) are 2515 to 2526 g.L^{-1} and two glasses from experiments at 2.0 GPa (1350, 1450°C) are 2542 and 2546 g.L^{-1}. There is no discernible systematic variation in density with run temperature; this is the expected consequence of all glass structures recording a similar T_g during quenching.

4.2.1. Molecular CO_2 extinction coefficient

The CO_2^{mol}/(CO_2^{mol} + carbonate) ratio was determined from the NMR spectra for samples synthesised at 2.0 GPa and 1300, 1350 and 1550°C. The ratios were combined with the total dissolved CO_2 data from bulk analysis to obtain the absolute concentration of CO_2^{mol} for these three glasses. The absorbance, thickness, molecular weight, measured glass density and this absolute concentration of CO_2^{mol} were then used to obtain the extinction coefficient of CO_2^{mol} species using Eqn. (3). The resulting values are not very accurate because the absolute concentration of CO_2^{mol} is very low (0.02 to 0.08 wt%) in the haplo phonolite. The values obtained for the linear extinction coefficients are 796 ± 250, 772 ± 250 and 875 ±

250 L.mol^{-1}.cm^{-1} at 1300, 1350 and 1550°C respectively. Given the large error, these values are in the same range as those determined for albite (945 L.mol^{-1}.cm^{-1}, Fine and Stolper, 1985) and rhyolite (1066 L.mol^{-1}.cm^{-1}, Blank, 1993). In subsequent calculations an average of all these values (890 L.mol^{-1}.cm^{-1}) will be assumed.

4.2.2. Carbonate extinction coefficient

The concentration of carbonate in each glass was obtained by subtracting the concentration of CO_2^{mol} (calculated from IR using the extinction coefficient of 890 L.mol^{-1}.cm^{-1}) from the total dissolved CO_2 concentration (from bulk analysis). The integral extinction coefficient (ε) was then calculated for the area of the carbonate doublet using the known concentration, density and molecular weight and the measured absorbance and thickness. The same spectrum of a volatile-free haplo-phonolite was subtracted from all CO_2-bearing spectra, but this appeared to fit the "background" equally well in all cases. As illustrated in Figure 5, the carbonate extinction coefficients derived in this way show surprisingly large systematic variations as a function of pressure and temperature. Figure 5a shows the extinction coefficient for the carbonate doublet as a function of run temperature for the 1.0 GPa experiments and similar trends are observed at other pressures. The calculated values of ε decrease from 1300 to 1450°C then increase to 1550°C and the magnitude of the change is larger than any possible error (for instance related to the background subtraction).

Figure 5b shows the change in calculated extinction coefficient as a function of run pressure for a temperature of 1550°C. It is important to note the decrease in the value of ε with increasing run pressure is far more significant than the change in glass density, which only varies by about 1% per 0.5 GPa. As with the run temperature-induced changes shown in Figure 5a, the changes in ε are larger than any error and are probably related to the change in relative abundance of different carbonate species as shown by IR data (figure 2b), with each subspecies of carbonate having its own value of ε. This explanation requires that differences in speciation must be retained to some extent through the quenching process, to give samples with different (but unresolved in the IR spectra) carbonate species and hence different average carbonate ε values (see section 4.3). An additional effect is that the viscosity of the melt probably decreases with increasing pressure (e.g., Kushiro, 1976). This would decrease Tg, and could explain why different relative concentrations of carbonate species with different extinction coefficients are present in the glasses quenched from different pressures.

It must therefore be concluded that IR is not currently a reliable method for determining CO_2 concentrations in glasses of 'intermediate' magma composition. It is clear that a more detailed comparison of NMR and IR spectra, in samples prepared at different conditions, is required to investigate this problem further.

4.3. Glass Versus Melt Speciation

The data from this study support previous observations (e.g. Stolper et al., 1987; Brooker et al., 1999) that the speciation preserved in CO_2-bearing glasses depends to some extent on the run temperature. This result is surprising, as any difference in the speciation at run conditions, should not be apparent in the glass structures. One would expect the speciation for all samples to be 'frozen in' at the same T_g because the quench rate for the piston cylinder apparatus does not vary significantly with run temperature. In this study it has also been found that the nature of the carbonate group (shown by Δv_3) and the carbonate IR extinction coefficient both depend on the run temperature. These two observations can be explained readily if (i) a range of carbonate species with a temperature dependent equilibrium are present in the melt; and (ii) the equilibrium is partially quenchable. The possibility of completely quenching the equilibrium species distribution from high-temperature seems very unlikely, as it implies some very slow exchange process in the melt. It is probable that only a relatively small fraction of the C-bearing species would have sufficiently slow

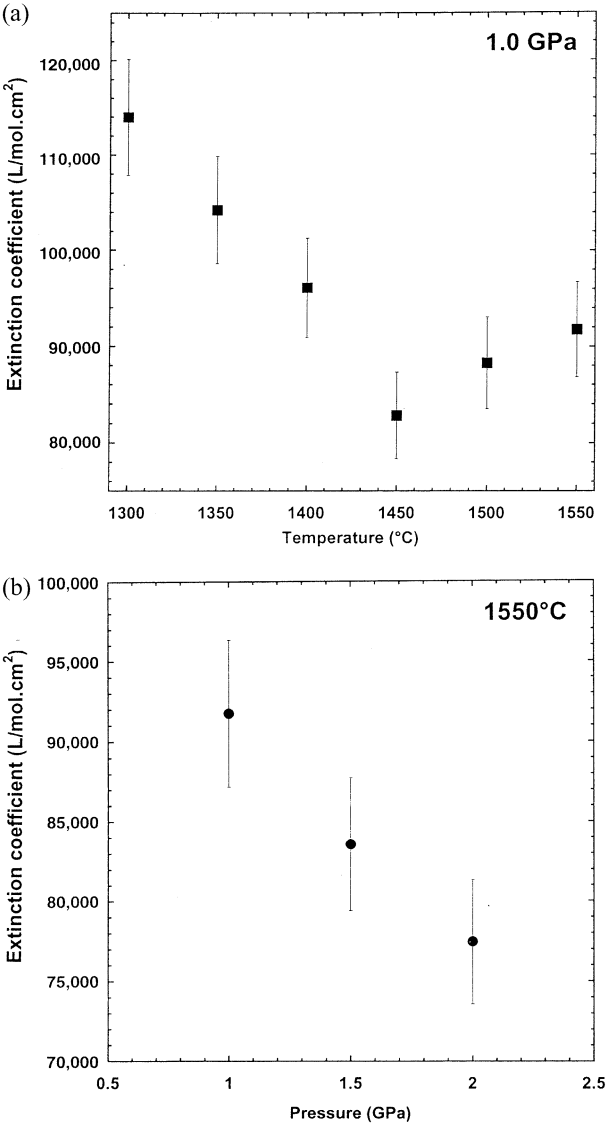

Fig. 5. The calculated integral extinction coefficients for the carbonate doublet plotted in a) as a function of temperature at 1.0 GPa, and in b) as a function of pressure at 1550°C. Error bars represent the range of values obtained for repeat analyses of the same sample.

kinetics. Although much more work is required to understand these effects in haplo-phonolite, new information on the temperature dependence of the speciation equilibrium has become available very recently, from annealing experiments on jadeite glass (Morizet et al., 2001). These results suggest that the relative concentration of CO_2^{mol} in silicate melts may be much higher than that observed in quenched glasses. Thus the slow exchange process, referred to above, might be related to a large activation energy for the conversion of CO_2^{mol} to one (or more) specific carbonate types during cooling. A higher CO_2^{mol} content in the haplo-phonolite melt is also one possible explanation for the relatively poor fit of the thermodynamically predicted solubility (Fig. 4) which is based on an assumption that the solubility mechanism is dominated by carbonate formation, as in Eqn. (1).

CONCLUSIONS

The solubility of carbon dioxide in a synthetic iron free phonolite melt has a positive pressure dependence and a variable, but negative temperature dependence consistent with the majority of recent studies on natural compositions. Solubility trends are in reasonable agreement with those for an Fe-bearing phonolite of Brooker et al. (2001a), but the replacement of FeO by MgO may have introduced some subtle differences in the carbonate complexation. A low solubility for CO_2 in phonolite, compared with potential parental compositions such as nephelinite (see Brooker et al, 2001a), implies that a high activity of CO_2, (and hence saturation) is easily reached by fractionation as well as decompression. Exsolution may give a suitable transport mechanism for magma ascent from the mantle, although any isobaric cooling may cause re-absorption of the exsolved fluid phase.

CO_2 speciation in phonolite glass is dominated by carbonate with several different types of complex being observed in both the FTIR and NMR spectra. Changes in the relative abundances of the different carbonate species as a function of equilibration pressure and temperature suggests the speciation in the melt may be significantly different from the glass with complex changes during quenching. This may be the cause of non-unique values of thermodynamic solubility parameters and IR extinction coefficients.

Acknowledgements—The authors are grateful to the University of Bristol and NERC for their financial support and to Dr. S. Kearns, Mr. M. Dury and Mr. F. Wheeler for their technical help. We also thank Penny King and two anonymous reviewers for their comments.

Associate editor: C. Romano

REFERENCES

Bailey D. K. (1980) Volcanism, earth degassing and replenished lithospheric mantle. *Phil. Trans. Roy. Soc. London, Series A* **297,** 309–322.

Bailey D. K. (1987) Mantle metasomatism-perspective and prospect. In *Alkaline Igneous Rocks* (eds. J.G. Fitton, and B.G.J. Upton) *Geol. Soc. Spec. Pub. No.* **30,** 1–13.

Bailey D. K. and MacDonald R. (1987) Dry peralkaline felsic liquids and carbon dioxide flux through the Kenya rift zone. In *Magmatic Processes: Physicochemical principles* (ed. B.O. Mysen) *Geochem. Soc. Spec. Pub.* **1,** 91–105.

Baker B. H. (1987) Outline of the petrology of the Kenya rift alkaline province. In *Alkaline Igneous Rocks* (eds. J. G. Fitton, and B. G. J. Upton) *Geol. Soc. Spec. Pub. No.* **30,** 293–311.

Bell K. and Keller J. (1995) Eds. Carbonatite volcanism of Oldoinyo Lengai and petrogenesis of natrocarbonatite. *IAVCEI Proceedings in Volcanology* **4,** Springer-Verlag. Berlin.

Blank J. G. (1993) An experimental investigation of the behavior of carbon dioxide in rhyolitic melt. Ph.D. thesis, California Institute of Technology.

Blank J. G. and Brooker R. A. (1994) Experimental studies of carbon dioxide in silicate melts: solubility, speciation and stable isotope behavior. In *Volatiles in Magmas*, (ed. M.R. Carroll & J.R. Holloway) *MSA Rev. Mineral.* **30,** 157–186.

Bottinga Y. and Javoy M. (1990) MORB degassing: Bubble growth and ascent. *Chem. Geol.* **81,** 255–270.

Brey G. P. (1976) CO_2 solubility and solubility mechanisms in silicate melts at high pressures. *Contrib. Mineral. Petrol.* **57,** 215–221.

Brey G. and Green D. H. (1975) The role of CO_2 in the genesis of olivine melilitites. *Contrib. Mineral. Petrol.* **49,** 93–103.

Brooker R. A., McMillan P. F., and Holloway J. R. (1992) The structural environment of C-N-O species dissolved in aluminosilicate melts by FTIR spectroscopy. *EOS* **73 (43),** 619.

Brooker R. A. (1998) The effect of CO_2 saturation on silicate-carbonate immiscible systems. *J. Petrol.* **39,** 1905–1915.

Brooker R. A., Holloway J. R., and Hervig R. L. (1998) Reduction in piston cylinder experiments: The detection of carbon infiltration into platinum capsules. *Am. Mineral.* **83,** 985–994.

Brooker R. A., Kohn S. C., Holloway J. R., McMillan P. F., and Carroll M. R. (1999) CO_2 solubility, speciation and dissolution mechanisms for melt compositions along the $NaAlO_2$-SiO_2 join. *Geochim. Cosmochim Acta* **63,** 3549–3565.

Brooker R. A., Kohn S. C., Holloway J. R., and McMillan P. F. (2001a) Structural controls on the solubility of CO_2 in silicate melts. Part I: Bulk solubility data. *Chem. Geol.* **174,** 225–240

Brooker R. A., Kohn, S. C., Holloway J. R., and McMillan P. F. (2001b) Structural controls on the solubility of CO_2 in silicate melts. Part II: IR characteristics of carbonate groups in silicate glasses. *Chem. Geol.* **174,** 241–254.

Coltorti M., Bonadiman C., Hinton R. W., Siena F., and Upton B. G. J. (1999) Carbonatite metasomatism of the oceanic upper mantle: Evidence from clinopyroxenes and glasses in ultramafic xenoliths of Grande Comore, Indian Ocean. *J. Petrol.* **40,** 133–165.

Dixon J. E. (1997) Degassing of alkalic basalts. *Am. Min.* **82,** 368–378.

Dixon J. E. and Pan V. (1995) Determination of the molar absorptivity of dissolved carbonate in basanitic glass. *Am. Mineral.* **80,** 1339–1342.

Dixon J. E. and Stolper E. M. (1995) An experimental study of water and carbon dioxide solubilities in mid-ocean ridge basaltic liquids. Part II: Application to Degassing. *J. Petrol.* **36,** 1633– 1646.

Draper D. S. and Green T. H. (1997) P-T phase relations of silicic alkaline, aluminous mantle xenolith glasses under anhydrous and C-O-H fluid saturated conditions. *J. Petrol.* **38,** 1187–1224.

Edgar A. D. (1987) The genesis of alkaline magmas with emphasis on source regions: inferences from experimental studies. In *Alkaline Igneous Rocks* (eds. J. G. Fitton, and B. G. J. Upton) *Geol. Soc. Spec. Pub. No.* **30,** 29–52.

Eggler D. H. (1989) Carbonatites, primary melts, and mantle dynamics. In *Carbonatites: Genesis and Evolution.* (ed. K. Bell) Unwin Hyman, London, pp 561–579.

Fine G. and Stolper E. (1985) The speciation of carbon dioxide in sodium aluminosilicate glasses. *Contrib. Mineral. Petrol.* **91,** 105–121.

Fogel R. A. and Rutherford M. J. (1990) The solubility of carbon dioxide in rhyolitic melts: A quantitative FTIR study. *Am. Mineral.* **75,** 1311–1326.

Freestone I. C. and Hamilton D. L. (1980) The role of liquid immiscibility in the genesis of carbonatites: an experimental study. *Contrib. Mineral. Petrol.* **73,** 105–17.

Frost D. J. and Wood B. J. (1995) Experimental measurements of the graphite C-O equilibrium and CO_2 fugacities at high-temperature and pressure. *Contrib. Mineral. Petrol.* **121,** 303–308.

Green D. H., Edgar A. D., Beasley P., Kiss E., and Ware N. G. (1974) Upper mantle source for some hawaiites, mugearites and benmoreites. *Contrib. Mineral. Petrol.* **48,** 33–43.

Haggerty S. E. (1989) Mantle metasomes and the kinship between carbonatites and kimberlites. In *Carbonatites: Genesis and Evolution.* (ed. K. Bell) pp 546–560 Unwin Hyman, London.

Hay D. E. and Wendlandt R. F. (1995) The origin of Kenya Rift Plateau-type flood phonolites: results of high-pressure/high-temperature experiments in the system phonolite-H_2O and phonolite-H_2O-CO_2. *J. Geophys. Res.* **100,** 401–410.

Holloway J. R. (1976) Fluids in the evolution of granitic magmas: consequences of finite CO_2 solubility. *Geol. Soc. Am. Bull.* **87,** 1513–1518.

Ihinger P. D., Hervig R. L., and McMillan, P. F. (1994) Analytical methods for volatiles in glasses. In *Volatiles in Magmas* (eds. M. R. Carroll & J. R. Holloway) *Rev. Mineral.* **30,** 67–121.

Johnson M. C., Anderson A. T., and Rutherford M. J. (1994) Pre-eruptive volatile contents of magmas. In *Volatiles in Magmas* (eds. M. R. Carroll & J. R. Holloway) *Rev. Mineral.* **30,** 281–330.

Kaszuba J. P. and Wendlandt R. F. (2000) Effects of carbon dioxide on dehydration melting reactions and melt compositions in the lower crust and the origin of alkaline rocks. *J. Petrol.* **41,** 363–386.

Kjarsgaard B. A. and Peterson T. D. (1991) Nephelinite-Carbonatite liquid immiscibility at Shombole volcano, East Africa: Petrographic and experimental evidence. *Mineral. Petrol.* **43,** 293–314.

Kohn S. C., Brooker R. A., and Dupree R. (1991) ^{13}C MAS NMR: A method for studying CO_2 speciation in glasses. *Geochim. Cosmochim. Acta* **55,** 3879–3884

Kubicki J. D. and Stolper E. M. (1995) Structural roles of CO_2 and $[CO_3]^{2-}$ in fully-polymerized, sodium aluminosilicate melts and glasses. *Geochim. Cosmochim. Acta* **59,** 683–698.

Kushiro I. (1976) Changes in viscosity and structure of melt of $NaAlSi_2O_6$ composition at high pressures. *J. Geophys. Res.* **81,** 6347–6350.

Laurora A., Mazzucchelli M., Rivalenti G., Vannucci R., Zanetti A., Barbieri M. A., and Cingolani C. A. (2001) Metasomatism and melting in carbonated peridotite xenoliths from the mantle wedge: The Gobernador Gregores case (Southern Patagonia). *J. Petrol.* **42,** 69–87.

Le Bas M. J. (1987) Nephelinites and carbonatites. In (Alkaline Igneous Rocks) (eds) Fitton, J.G. and Upton, B.G.J., Geological Society Special Publication N° 30. pp 53–83.

Lippard S. J. (1973) The petrology of phonolites from the Kenya Rift. *Lithos* **6,** 217–234.

Maekawa H., Maekawa T., Kawamura K., and Yokokawa T. (1991) The structural groups of alkali silicate glasses determined from ^{29}Si MAS NMR. *J. Non-Cryst. Solids* **127,** 53–64.

McInnes B. I. A. and Cameron E. M. (1994) Carbonated, alkaline hybridizing melts from a sub-arc environment: mantle wedge samples from the Tabar-Lihir-Tanga-Feni arc, Papua new Guinea. *Earth Planet. Sci. Lett.* **122,** 125–141.

Morizet Y., Kohn S. C., and Brooker R. A. (2001) Annealing experiments on CO_2-bearing jadeite glass: An insight into the true temperature dependence of CO_2 speciation in silicate melts. *Min. Mag.* **65,** 701–707.

Mysen B. O. (1976) The role of volatiles in silicate melts: solubility of carbon dioxide and water in feldspar, pyroxene and feldspathoid melts to 30kb and 1625°C. *Am. J. Sci.* **276,** 969–996.

Mysen B. O. (1988) Structure and properties of silicate melts. Developments in Geochemistry, 4. Elsevier. Amsterdam. 354p.

Mysen B. O. and Virgo D. (1980a) The solubility behavior of CO_2 in melts on the join $NaAlSi_3O_8$-$CaAl_2Si_2O_8$-CO_2 at high pressure and temperature: a Raman spectroscopic study. *Amer. Mineral.* **65,** 1166–1175.

Mysen B. O. and Virgo D. (1980b) Solubility mechanisms of carbon dioxide in silicate melts: a Raman spectroscopic study. *Amer. Mineral.* **65,** 885–899.

Mysen B. O., Arculus R. J., and Eggler D. H. (1975) Solubility of carbon dioxide in natural nephelinite, tholeiite and andesite melts to 30 kbar pressure. *Contrib Mineral Petrol* **53,** 227– 239.

Mysen B. O., Eggler D. H., Seitz M. G., and Holloway J. R. (1976) Carbon dioxide in silicate melts and crystals. Part 1; Solubility measurments. *Am. J. Science* **276,** 455–479.

Pan V., Holloway J. R., and Hervig R. L. (1991) The pressure and temperature dependence of carbon dioxide solubility in tholeiitic basalt melts. *Geochim. Cosmochim. Acta* **55,** 1587– 1595.

Price R. C. and Green D. H. (1972) Lherzolite nodules in a 'mafic phonolite' from north-east Otago, New Zealand. *Nat. Phys. Sci.* **235,** 133–134.

Rai C. S., Sharma S. K., Muenow D. W., Matson D. W., and Byers C. D. (1983) Temperature dependence of CO_2 solubility in high pressure quenched glass of diopside composition. *Geochim. Cosmochim. Acta* **47,** 953–958.

Saxena, S. K. and Fei, Y. (1987) High pressure and high temperature fluid fugacities. *Geochim. Cosmochim. Acta* **51,** 783–791.

Sharma S. K. (1979) Structures and solubility of carbon dioxide in silicate glasses of diopside and sodium melilite composition at high pressures from Raman spectroscopic data. *Carnegie Inst. Wash. Yrbk.* **78,** 537–542.

Sparks R. S. J., Barclay J., Jaupart C., Mader H. M., and Phillips J. C. (1994) Physical aspects of magma degassing I. Experimental and theoretical constraints on vesiculation. In *Volatiles in Magmas, (ed. M.R. Carroll & J.R. Holloway) MSA Rev. Mineral.* **Vol 30,** 413–445.

Stolper E., Fine G., Johnson T., and Newman S. (1987) Solubility of carbon dioxide in albitic melt. *Am. Mineral.* **72,** 1071–1085.

Stolper E. and Holloway J. R. (1988) Experimental determination of the solubility of carbon dioxide in molten basalt at low-pressure. *Earth Planet. Sci. Lett.* **87,** 397–408.

Taylor W. R. (1990) The dissolution mechanism of CO_2 in aluminosilicate melts: Infrared spectroscopic constraints on the cationic environments of dissolved $[CO_3]^{2-}$. *Eur. J. Min.* **2,** 547–563.

Tossell J. A. (1995) Calculation of the ^{13}C NMR shieldings of the CO_2 complexes of aluminosilicates. *Geochim. Cosmochim. Acta* **59,** 1299–1305.

Thibault Y. and Holloway J. R. (1994) Solubility of CO_2 in a Ca-rich leucitite: Effects of pressure, temperature, and oxygen fugacity. *Contrib. Mineral. Petrol.* **116,** 216–224.

Verweij H., van den Boom H., and Breemer R. E. (1977) Raman scattering of carbonate ions dissolved in potassium silicate glasses. *J. Am. Chem. Soc.* **60,** 529–534.

Wallace M. E. and Green D. H. (1988) An experimental determination of primary carbonatite magma compositions. *Nature* **335,** 343–346

Watson E. B. (1994) Diffusion in volatile-bearing magmas. In *Volatiles in Magmas* (eds. M.R. Carroll & J.R. Holloway) *Rev. Mineral.* **30,** 371–411.

Wright J. B. (1966). Olivine nodules in a phonolite of the East Otago alkaline province, New Zealand. *Nature* **210,** 519.

Wright J. B. (1969) Olivine nodules and related inclusions in trachyte from the Jos Plateau, Nigeria. *Min. Mag.* **37,** 370–374.

Yaxley G. M. and Kamenetsky V. (1999) In situ origin for glass in mantle xenoliths from southeastern Australia: insights from trace element compositions of glasses and metasomatic phases. *Earth Planet. Sci. Lett.* **172,** 97–109.

Yokokawa T., Kawamura K., Maekawa H., and Sawaguchi N. (1999) Equilibrium of $O^2 + O^0 = 2O^-$ in oxide melts; examinations of its reality by three approaches. *J. Mol. Liq.* **83,** 311–321.

Appendix

Sample	Mass of analyzed sample (mg)	wt.% CO_2
	1.0 GPa, 1300°C, Weighted solubility = 0.78 wt.%CO_2	
YP12	104.69, 54.59, 38.42	0.78, 0.78, 0.79
	1.0 GPa, 1350°C, Weighted solubility = 0.65 wt.%CO_2	
YP34	40.4, 29.9, 63.4	0.66, 0.69, 0.62
	1.0 GPa, 1400°C, Weighted solubility = 0.73 wt.%CO_2	
YP10	103.16, 56.35	0.70, 0.79
	1.0 GPa, 1450°C, Weighted solubility = 0.67 wt.%CO_2	
YP35	28.3, 29.1, 46.1	0.70, 0.64, 0.67
	1.0 GPa, 1500°C, Weighted solubility = 0.72 wt.%CO_2	
YP07	100.8, 41.63	0.72, 0.72
	1.0 GPa, 1550°C, Weighted solubility = 0.75 wt.%CO_2	
YP39	93.86, 19.73	0.75, 0.75
	1.5 GPa, 1300°C, Weighted solubility = 1.41 wt.%CO_2	
YP11	121.96, 51.57, 60.62	1.42, 1.39, 1.39
	1.5 GPa, 1350°C, Weighted solubility = 1.12 wt.%CO_2	
YP31	50.38, 45.56, 66.1	1.09, 1.14, 1.14
	1.5 GPa, 1400°C, Weighted solubility = 1.17 wt.%CO_2	
YP09	117.47, 62.07, 68.85	1.18, 1.15, 1.18
	1.5 GPa, 1450°C, Weighted solubility = 1.06 wt.%CO_2	
YP32	49.68, 47.55, 76.81	1.07, 1.13, 1.02
	1.5 GPa, 1500°C, Weighted solubility = 1.10 wt.%CO_2	
YP06	111.56, 52.63, 71.03	1.11, 1.11, 1.09
	1.5 GPa, 1550°C, Weighted solubility = 1.08 wt.%CO_2	
YP33	34.1, 40.18, 66.7	1.10, 1.05, 1.08
	2.0 GPa, 1300°C, Weighted solubility = 1.99 wt.%CO_2	
YP01	102.41, 61.48, 70.88	1.96, 1.95, 1.95
YP04	108.76	1.87
YP22	31.66, 32.06, 41.48, 32.45	2.01, 1.93, 1.94, 1.93
YP27	24.85, 39.38, 39.99, 21.5, 34.78	2.01, 2.22, 2.06, 2.14, 2.23
YP46	24.51, 27.57	1.92, 2.14
	2.0 GPa, 1350°C, Weighted solubility = 1.90 wt.%CO_2	
YP28	51.85, 50.76, 62.53	1.96, 1.88, 1.88
	2.0 GPa, 1400°C, Weighted solubility = 1.66 wt.%CO_2	
YP02	105.84, 50.77, 83.88	1.65, 1.56, 1.63
YP66	84.4, 103.4, 28.0	1.66, 1.69, 1.83
	2.0 GPa, 1450°C, Weighted solubility = 1.78 wt.%CO_2	
YP29	52.78, 44.23, 78.92	1.86, 1.76, 1.74
	2.0 GPa, 1500°C, Weighted solubility = 1.56 wt.%CO_2	
YP03	103.5, 48.29	1.55, 1.59
	2.0 GPa, 1550°C, Weighted solubility = 1.65 wt.%CO_2	
YP30	52.57, 36.8, 76.64	1.63, 1.68, 1.64
	2.5 GPa, 1300°C, Weighted solubility = 2.77 wt.%CO_2	
YP48	23.84, 44.86	2.80, 2.76
	2.5 GPa, 1350°C, Weighted solubility = 2.46 wt.%CO_2	
YP62	40.7	2.46
	2.5 GPa, 1400°C, Weighted solubility = 2.29 wt.%CO_2	
YP50	16.22, 17.29	2.25, 2.34
	2.0 GPa, 1500-1400°C, Weighted solubility = 1.74 wt.%CO_2	
YP20	101.36, 49.07, 54.45	1.76, 1.72, 1.72
	2.0 GPa, 1300-1400°C, Weighted solubility = 1.93 wt.%CO_2	
YP21	100.79, 49.45, 83.58	1.90, 1.97, 1.95
	1.5 GPa, 1300°C, Natural phonolite, Weighted solubility = 0.85 wt.%CO_2	
YP60	42.1	0.85
	1.0 GPa, 1300°C, Natural phonolite, Weighted solubility = 0.56 wt.%CO_2	
YP61	44.5	0.56